Thin-Walled Structures **18** (1994) 97–116

Local Buckling Experiments on FRP Columns

John Tomblin & Ever Barbero

Mechanical and Aerospace Engineering, Constructed Facilities Center, West Virginia University, Morgantown, WV 26506-6101, USA

(Received 31 July 1991; revised version received 3 March 1992; accepted 16 June 1992)

ABSTRACT

In this paper, local flange-buckling of thin-walled pultruded FRP columns is investigated. Experimental data are presented and correlated with theoretical predictions. Good agreement between theoretical and experimental results is found. Possible explanations for slight deviations in the experimental data are advanced. The experimental and data reduction procedures used to obtain the local buckling loads are presented. A new data reduction technique using Southwell's method is developed to interpret local buckling test data. The usefulness of the data reduction technique is demonstrated for various column sections and experimental conditions.

1 INTRODUCTION

Pultruded composite beams and columns are being extensively used for civil engineering structural applications. They have many advantages over conventional materials (steel, concrete, wood, etc.), such as light weight and high corrosion resistance. Mass production of composite structural members (e.g. by pultrusion) makes composite materials cost-competitive with conventional ones. In the pultrusion process, fibers and polymer resin are pulled through a heated die that provides the shape of the cross-section to the final product. Pultrusion is a continuous process for the production of prismatic sections of virtually any shape.[1] Other mass production techniques like automatic tape layout can also be used to produce prismatic sections.

Thin-Walled Structures 0263-8231/94/$07·00

Pultruded structural members have open or closed thin-walled cross-sections. For long composite columns, overall (Euler) buckling is more likely to occur before any other instability failure. For short columns, local buckling occurs first, leading either to large deflections and finally to overall buckling or to material degradation due to large strains (crippling). For intermediate lengths, interaction between local and global buckling and possibly material degradation may occur. Because of the large elongation to failure allowed by both the fibers and the resin, the composite material remains linearly elastic for large deflections and strains, unlike conventional materials that yield (steel) or crack (concrete) for moderate strains. Therefore, buckling is the governing failure for this type of cross-section and the critical buckling load is directly related to the carrying capacity of the member.

For a composite column, the classical buckling theory[2] in combination with basic concepts of the classical lamination theory[3,4] are applied in order to determine the bending stiffness of the column[5] and the critical buckling load.[6] In the case of short columns, Euler's theory cannot be applied because short column buckling failure is associated more likely with local buckling (i.e. buckling of a part of the cross-section of the column) or material failure that may be encountered before any instability failure. A very short column of solid cross-section with thin parts, such as wide flange I-beams and box beams, is considered herein.

The problem of local buckling has already been considered for steel cross-sections and considerable research has been done in this area in order to increase the carrying capacity of a steel member against local buckling by introducing stiffeners.[7] An analytical solution for local buckling of pultruded composite columns[6] is used in this work. Other alternatives are to use the Finite Strip method[8] or the Finite Element Method.[9] Experimental results on FRP columns for cooling towers were presented by Yuan.[10]

In almost any experimental test, the validity of the test somewhat relies on the workmanship of the testing apparatus and material being tested. This is particularly true in a buckling test where a high state of instability exists. Due to the manufacturing process of pultruded fiber reinforced plastic (FRP) beams, imperfections in the final beam composition are impossible to control to any reliable estimate. These imperfections will play a large role in any buckling experiment.

2 DATA REDUCTION IN LONG-COLUMN BUCKLING

This section provides the background for the proposed data reduction method for local buckling described in Section 3. In any buckling experi-

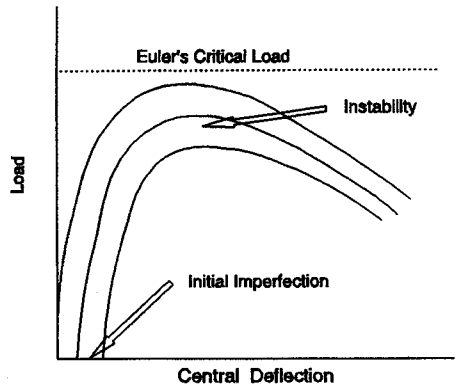

Fig. 1. Experimental curves for a column with initial imperfections.

ment, particularly one using FRP sections, the theoretical critical load of the column is almost never achieved due to material imperfections. The resulting load–deflection curve will have the form represented in Fig. 1. Its maximum is very difficult to obtain experimentally and it may not have a close correspondence with the theoretical critical load P_{cr}. Thus, it becomes necessary to make use of the method proposed by Southwell[11, 12] which takes into account the load reduction resulting from such imperfections.

2.1 Southwell's method

The governing equation for an axially loaded column in terms of the deflection w and an imperfection w_o, both measured from the line of application of the load, is

$$D\left(\frac{d^2w}{dx^2} - \frac{d^2w_o}{dx^2}\right) + Pw = 0 \tag{1}$$

Provided that w_o vanishes at each end of the column, a general solution of eqn (1) may be obtained by expressing w and w_o in terms of a Fourier series, assuming w and w_o will be continuous functions of x:

$$w = \sum_{n=1}^{\infty}\left[A_n \sin\frac{n\pi x}{L}\right] \tag{2}$$

$$w_o = \sum_{n=1}^{\infty}\left[\overline{A_n} \sin\frac{n\pi x}{L}\right] \tag{3}$$

By substituting eqn (2) and (3) into eqn (1), the following relation is found:

$$A_n = \frac{\overline{A_n}}{1 - \dfrac{P}{P_n}} \tag{4}$$

where P_n represents the critical load of the nth mode. The true deflection measured with respect to the centroidal axis of the column (or middle surface of the flange) is $\Delta = w - w_0$. In the case of no interaction among modes, one modes dominates and Δ reduces

$$\Delta = \frac{\overline{A_1} \sin \dfrac{\pi x}{L}}{\dfrac{P_1}{P} - 1} \tag{5}$$

or

$$\frac{\Delta}{P} = \frac{1}{P_1} \Delta + \frac{\overline{A_1}}{P_1} \sin \frac{\pi x}{L} \tag{6}$$

Equation (5) relates the deflection Δ to the increasing load P. This equation also represents a rectangular hyperbola having the axis $\Delta = -\overline{A_1}$ and the horizontal line $P = P_1$ as asymptotes (Fig. 2). Equation (6) represents a linear relationship between Δ/P and Δ with the inverse of the slope representing the critical buckling load and the Δ-intercept representing the apparent imperfection (Fig. 3).

Southwell's method may also be extended to cases which also take into account real imperfections of the beam, eccentricity at the ends, the beam's own weight, and transverse lateral load,[13, 14] all of which have the same effect when analyzed by Southwell's method. On all accounts, the load will not pass exactly through the centroid of the section and the column will be subjected to bending actions and lateral deflections from the first application of load. Southwell's method is extended in the next section for data reduction of local-buckling test data.

3 DATA REDUCTION IN LOCAL BUCKLING

Although Southwell's method was developed for the long column (Euler) case, application to short columns, tested in the manner described above, appears to be possible. As will be seen in following sections, measurements taken on the flanges during a local buckling test fall on the same hyperbolic curve as shown in Fig. 2. Thus, when this curve is linearized, the slope of the resulting straight line will give the inverse of the critical load as shown in Fig. 3.

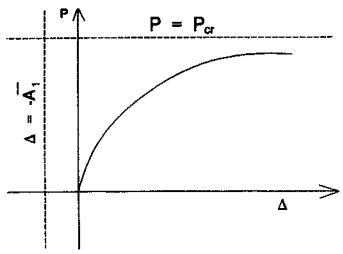

Fig. 2. Hyperbolic Δ–P plot with asymptotes $P = P_1$ and $\Delta = -\overline{A_1}$.

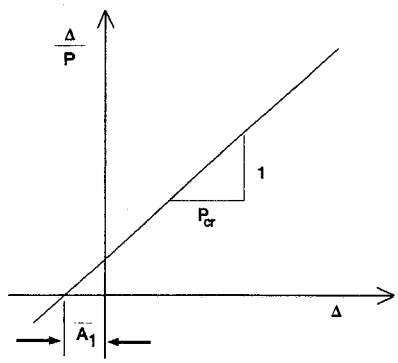

Fig. 3. Linearized Δ–Δ/P plot with slope $1/P_1$ and intercept $-\overline{A_1}$.

A major question in the application of the proposed data reduction method to the local buckling measurement is the placement of the gauges with respect to the buckled mode shape. As in the classical Southwell's method, the most logical gauge placement will be in the center of a buckling wave in the sample being tested (where the maximum deflection can be obtained with respect to the compressive load). But, in local flange buckling tests, the convenience of being able to properly place a gauge in the center of a wavelength is impossible due to the unknown buckled shape.

For example, a typical buckled flange with three gauges placed along the wavelength L' is shown in Fig. 4. Recalling eqn (6), the deflection is dependent upon the position x of the gauge with respect to the wavelength L'. Hence, with respect to Fig. 4, eqn (6) becomes

$$\frac{\Delta}{P} = \frac{1}{P_1}\Delta + \frac{\overline{A_1}}{P_1}\sin\frac{\pi x}{L'} \tag{7}$$

When this linear relation is plotted, the slope of the straight line is the inverse of the critical load $(1/P_1)$ and the intercept is the initial deflection

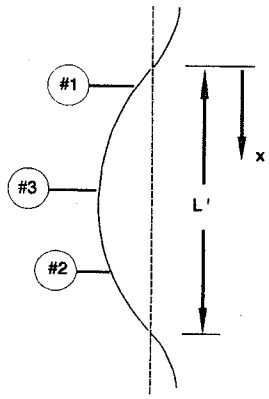

Fig. 4. Section of buckled flange with wavelength L''.

or imperfection, in this case $\overline{A_1}\sin(\pi x/L)$. When several gauges from the same test are linearized and placed on the Δ–Δ/P plot, the resulting lines will fall on lines similar to those represented in Fig. 5.

As shown in Fig. 5, even though all lines have different intercepts (different values of the wavelength position x), the slope remains constant at $1/P_1$. Hence, the critical load can be obtained regardless of the gauge position with respect to the wavelength. This is very important because of the following: if only one displacement transducer is available, its output can be used regardless of its location with respect to the unknown location of the maximum deflection of the buckled flange. If several displacement transducers are available, their output can be used without further complications introduced by the uncertainty of wavelength and wave location. It should be noted that the quantity $\overline{A_1}\sin(\pi x/L)$ will be very

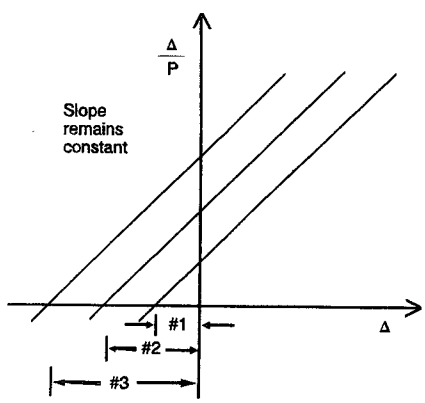

Fig. 5. Linearized plot showing slope independence with respect to dial gauge placement.

small due to the fact that the initial deflection is not apparent in the column, but initial imperfections in the material exist. It should also be noted that in the extreme case when little or no measurement is recorded, the gauge may be positioned at inflection point $x = 0$ or L. In this case, the measurements taken from the gauge should be neglected for the Southwell analysis.

4 ANALYSIS OF EXPERIMENTS

Local flange buckling of an axially compressed column plays an important role in the load carrying capacity of the member. Since deformations in the flange during local buckling can be quite large, they can induce material damage. Therefore, the local buckling load can be used as a failure criterion for the entire column.

In this section, the local flange buckling behavior of pultruded composite wide flange I-beams is studied. A theoretical orthotopic plate model based on the Levy method with one free and one elastically restrained edge was used to predict the behavior of the test specimens.[6] For each section being tested, three cases were considered for the elastic spring constant d representing the amount of elastic support provided by the web: clamped ($d \to \infty$), elastic ($d = D_{22}^{\mathrm{WEB}}$) and hinged ($d = 0$). As shown by Raftoyiannis,[15] the elastic supported boundary condition $d = D_{22}^{\mathrm{WEB}}$ best approximates the true boundary conditions which exist in the wide flange I-beam. Thus, any experimental loads will be compared to the elastically restrained case.

In addition to the theoretical curves, numerous experimental tests were performed on each wide flange I-beam section. At least three tests were done on each section with lengths corresponding to mode II, III and IV of the theoretical local buckling curves. Dial gauges were placed along the flanges and measurements of the flange deflection and load were obtained. A scheme based on Southwell's method, as described in Section 3, was used to reduce the data and determine the critical load. All experimental loads appear to be in good agreement with the theoretical predicted value.

4.1 Experimental setup and procedure

The flange local buckling tests were performed using a Baldwin test machine to apply the axially compressive load to the specimens. Various column lengths were cut, depending on the specific section being tested. The FRP beam specimens were manufactured and supplied by Creative Pultrusions, Inc.[1] Local buckling tests were conducted using the following

doubly-symmetric wide flange I-beams: 102 mm × 102 mm × 6·4 mm (4″ × 4″ × 1/4″); 152 mm × 152 mm × 6·4 mm (6″ × 6″ × 1/4″); 152 mm × 152 mm × 9·5 mm (6″ × 6″ × 3·8″) and 203 mm × 203 mm × 9·5 mm (8″ × 8″ × 3/8″). Table 1 shows the flange properties for each FRP section along with the elastic support provided by the web. Using the properties for each section, Figs. 6–9 show the theoretical buckling curves predicted by the Levy solution[6] along with the overall (Euler) buckling curves. Note that in Figs 6–9, the plots were nondimensionalized by the flange width and the local buckling load (listed below in Tables 2–4) for each section.

Since all the lengths and sections were to be loaded into compression, it was very important to check that all cuts made were perpendicular to the column length. This was done to ensure that the cross-section was loaded uniformly.

To distribute a uniform load from the Baldwin machine, a thick steel plate was used at both ends. In addition to the steel plate, a protective grid constructed from 25·4 mm (1″) steel square bar was mounted to the plate.

TABLE 1

Flange Properties and Web Support for Each Wide-Flange I-Beam Section (note: $D_{16} = D_{26} = 0$ for all flanges

Section (mm)	D_{11} *(N cm)* $[\times 10^3]$	D_{12} *(N cm)* $[\times 10^3]$	D_{22} *(N cm)* $[\times 10^3]$	D_{66} *(N cm)* $[\times 10^3]$	D_{22}^{WEB} *(N cm)* $[\times 10^3]$
102 × 102 × 6·4	45·04	8·218	20·88	6·664	20·74
152 × 152 × 6·4	48·46	9·121	22·92	7·248	21·05
102 × 102 × 9·5	157·1	26·71	68·71	22·23	67·11
203 × 203 × 9·5	161·3	26·82	69·09	22·39	67·52

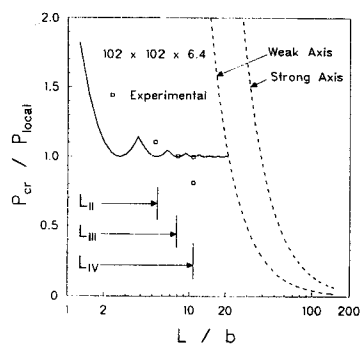

Fig. 6. Experimental loads for modes II, III and IV compared with theoretical curves for the 102 mm × 102 mm × 6·4 mm (4″ × 4″ × 1/4″) WF I-beam.

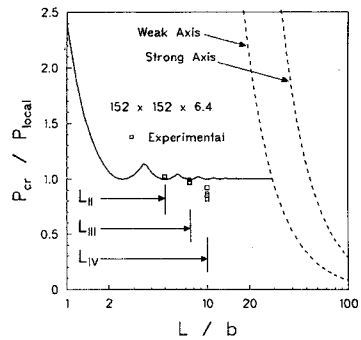

Fig. 7. Experimental loads for modes II, III and IV compared with theoretical curves for the 152 mm × 152 mm × 6·6 mm (4″ × 6″ × 1/4″) WF I-beam.

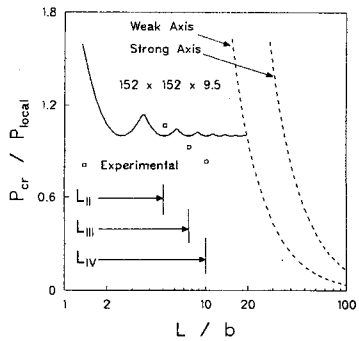

Fig. 8. Experimental loads for modes II, III and IV compared with theoretical curves for the 152 mm × 152 mm × 9·5 mm (6″ × 6″ × 3/8″) WF I-beam.

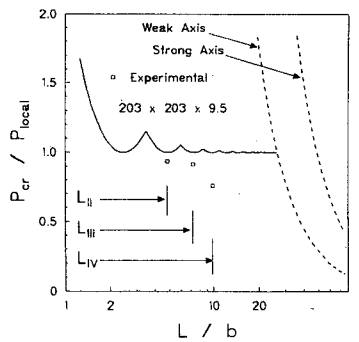

Fig. 9. Experimental loads for modes II, III and IV compared with theoretical curves for the 203 mm × 203 mm × 9·5 mm (8″ × 8″ × 3/8″) WF I-beam.

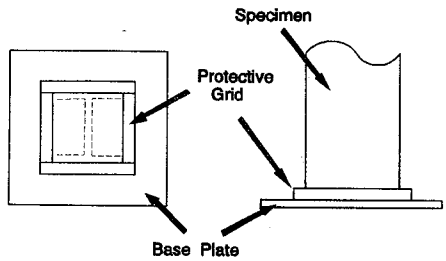

Fig. 10. Experimental setup showing base plate and protective grid.

This protective grid surrounds the specimen on all sides, as shown in Fig. 10, to protect against lateral slippage. It should be noted that the protective grid does not allow free rotation at the ends of the column but was needed for safety reasons. Hence, the boundary conditions are slightly different than the simply supported case assumed in the theoretical analysis.

Dial gauges, with 0·025 mm (0·001″) accuracy and a maximum measurement of 25·4 mm (1″), were used to detect the deflection of the flanges. An average of four dial gauges were placed along the specimen length attached to the outer edge of the flange. Figure 11 shows a typical dial gauge placement along the specimen length. As seen from Fig. 11, the dial gauges were staggered on both sides of the flanges along the length of the column. Since the exact shape and mode of the deflected flange are unknown, the exact longitudinal placement of the gauges was determined randomly in a staggered pattern as indicated above. All dial gauges were then placed into position and preset to a reading of approximately 12·7 mm (0·5″). This presetting was done to allow the deflection of the flange to be positive or negative, as measured by the dial gauge, since the shape, inflection and mode of the flange is an unknown.

The testing procedure consisted of loading the column and periodically taking measurements from the dial gauges. In the initial phases of the tests, the stepsize of the readings somewhat depended upon the theoretically predicted local buckling load (22 kN to 44 kN stepsize). Once a noticeable change occurred in the gauges, the stepsize in the gauge readings was decreased. It was also noticed that in the very initial stages of the tests ($P < 111$ kN), the gauge readings fluctuated slightly. These changes are not considered as buckling, but as deformations occurring while the column was being loaded as a result of initial imperfections. Once a certain load was reached (around $P = 120$ kN), the gauges stabilized and did not move until the approach of the local buckling load. It should be noted that these initial imperfections were not consistent in all specimens

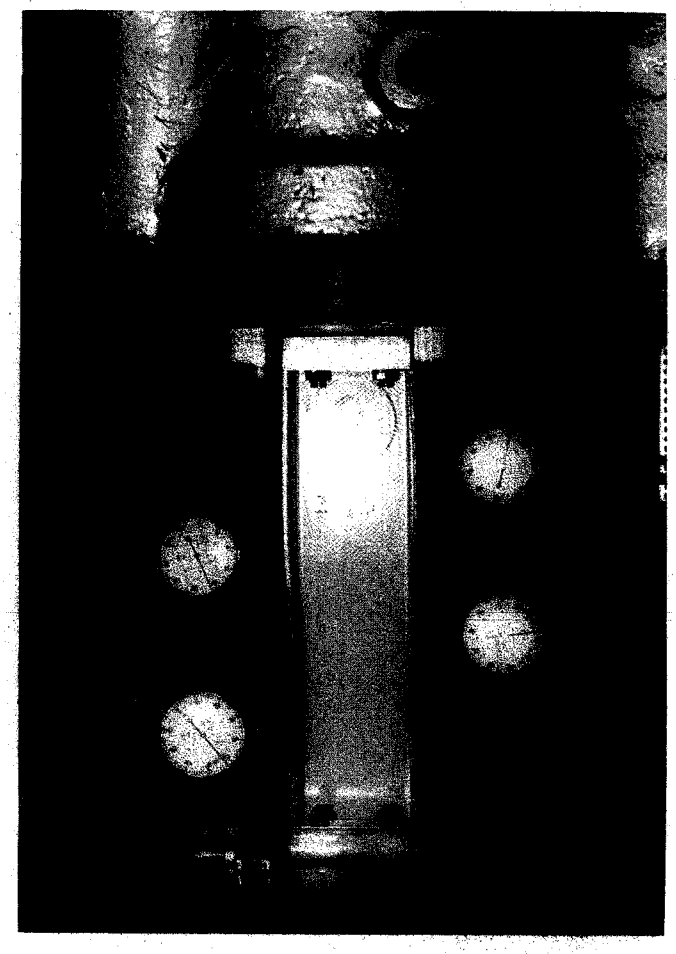

Fig. 11. Typical dial gauge placement along WF I-beam flanges (actual test shown for the 102 mm × 102 mm × 6·4 mm (4″ × 4″ × 1/4″) WF I-beam).

that were tested (some specimens stabilized at or below 22 kN). All specimens stabilized over an ample range of loads (133 kN to 445 kN range). Hence, all measurements taken before the stabilized period were neglected for the buckling analysis.

Almost all specimens were loaded and measurements taken until the flange was clearly buckled by eyesight. Once the final readings were taken, the column was unloaded. It should also be noted that in most tests, cracking of various kinds occurred inside the columns during the test. Thus, any attempt to reload the specimen to repeat the test will result in lower readings for the local buckling load than in the initial test when the material is undamaged.

4.2 Experimental test results

Local flange buckling tests were conducted on the wide flange I-beams listed in Section 4.1. At least three tests were done on each section. The lengths that were tested corresponded to the theoretical length calculated for a local buckling mode of II, III and IV. During each test, dial gauge measurements were taken from each gauge. The results were then plotted on a Δ–P plot, in which a hyperbolic relation was obtained (see Section 2). This curve was then linearized on a Δ–Δ/P, in which a linear regression was done on each separate gauge measurement (see Section 3). The average correlation coefficient calculated for each gauge measurement for all local buckling tests was 0·99. The resulting slopes and intercepts (regression coefficients) were averaged to obtain a general slope for the test. The resulting critical buckling load was then determined from the inverse of the average slope. The deviation of the average regression line with respect to the individual regression line for a single gauge (for each single test) was less than 1% for all tests. Hence, averaging of the slopes obtained from each gauge introduced a negligible error in the buckling load. For plotting purposes, the intercepts were also averaged in order that all gauge measurements and the average regression line could be shown on a single plot for one local buckling test. The average intercept for the test introduced virtually no change in any regression line with respect to the original line due to the extremely small magnitude of the intercept value (small imperfection).

4.2.1 Mode II results

The shortest lengths that were tested in the short column tests were lengths corresponding to a local buckling mode II. For the theoretical mode II lengths, the buckled flange will have a shape corresponding to two full wavelengths. Figures 6–9 show the mode II lengths as determined from each of the theoretical curves generated in Section 4.1, corresponding to each wide flange I-beam. Figures 12–14 show the gauge measurements taken during the test and the resulting linear regressed line corresponding to three of the wide flange I-beam sections tested. These three examples show the behaviors observed throughout the experimental program. As seen from Figs 12–14, all gauge measurements have a hyperbolic relationship and a resulting linear relationship for Δ and Δ/P. The extent of the hyperbolic relationship was dependent on the amount of imperfection existing in the material and varied from test to test. Table 2 shows the length, theoretical buckling load, experimental buckling load (inverse of the slope) and the percentage difference between the theoretical and

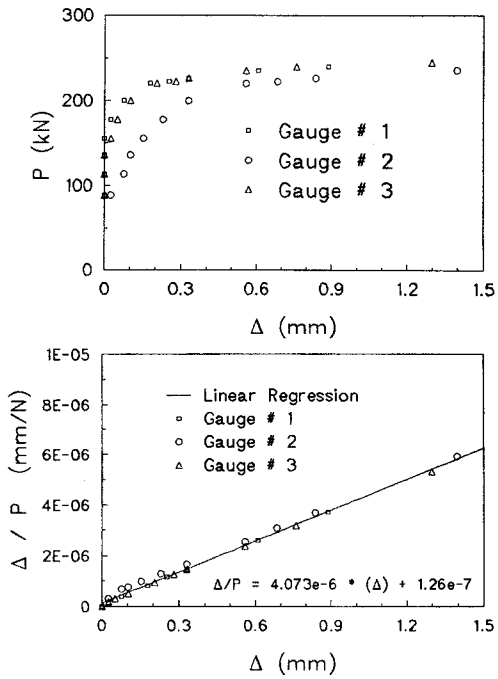

Fig. 12. Mode II hyperbolic and linearized measurements for the 102 mm × 102 mm × 6·4 mm (4″ × 4″ × 1/4″) WF I-beam.

experimental loads for each section tested. As seen from Table 2, the percentage error is less than 11% for all sections tested. With the exception of the 203 mm × 203 mm × 9·5 mm (8″ × 8″ × 3/8″), which may be due to a large imperfection, all experimental loads are slightly higher than the theoretical value. This larger load and percentage error obtained could be a direct result of the boundary conditions assumed in the theoretical analysis. As stated before, the theoretical analysis[6] assumes simply-supported boundary conditions at the ends. The boundary conditions in the test were not simply-supported but a combination of fixed and simply-supported. This boundary condition difference can explain the higher load obtained experimentally.

4.2.2 Mode III results

The next lengths that were tested corresponded to mode III lengths, shown in Figs 6–9, as taken from the theoretical curves for each section tested. For the theoretical mode III lengths, the buckled flange will have a shape corresponding to three full wavelengths. Figure 15 shows the hyperbolic measurements taken during the test of the

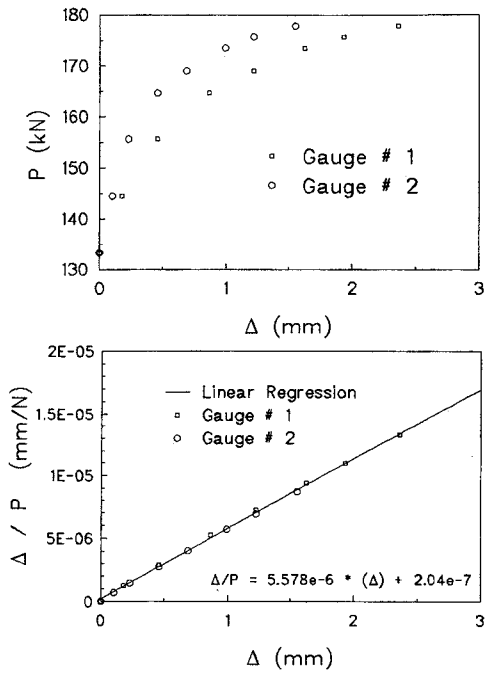

Fig. 13. Mode II hyperbolic and linearized measurements for the 152 mm × 152 mm × 6·4 mm (6″ × 6″ × 1/4″) WF I-beam.

TABLE 2
Resulting Experimental Local Buckling Loads for Mode II Tests

Section (mm)	*Length (cm)*	P_{theory} *(kN)*	$P_{exper.}$ *(kN)*	*% Diff.*
102 × 102 × 6·4	26·7	223·5	246·6	10·3
152 × 152 × 6·4	38·1	175·3	179·0	2·1
152 × 152 × 6·4	38·1	175·3	179·3	2·3
152 × 152 × 9·5	39·4	547·5	583·9	6·7
203 × 203 × 9·5	49·5	434·4	406·1	6·5

152 mm × 152 mm × 6·4 mm (6″ × 6″ × 1/4″) wide flange I-beam and the resulting linear regressed line. Table 3 shows the length, theoretical buckling load, experimental buckling load (inverse of slope) and the percentage difference between experimental and theoretical loads. As seen in Table 3, all differences were less than 9% and all loads were slightly lower than the theoretical (which could result from material imperfection). It should also be noted that both the 102 mm × 102 mm × 6·4 mm (4″ × 4″ × 1/4″) and the 152 mm × 152 mm × 6·4 mm (6″ × 6″ × 1/4″) tests result in errors less than 4%, thus proving the accuracy of the theoretical values.

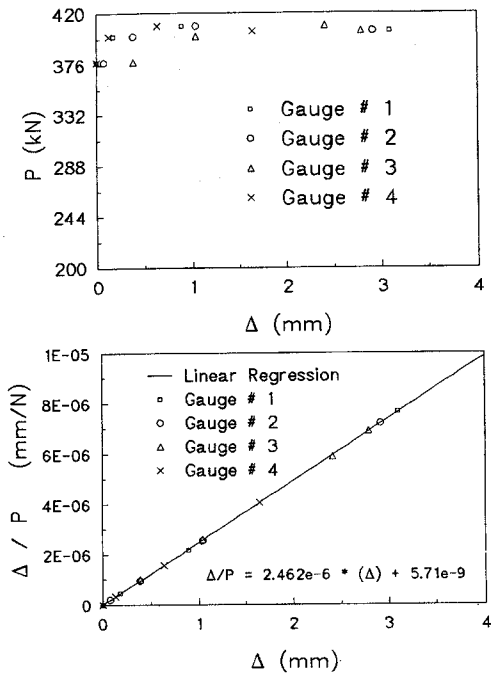

Fig. 14. Mode II hyperbolic and linearized measurements for the 203 mm × 203 mm × 9·5 mm (8″ × 8″ × 3/8″) WF I-beam.

TABLE 3
Resulting Experimental Local Buckling Loads for Mode III Tests

Section (mm)	*Length (cm)*	P_{theory} *(kN)*	$P_{exper.}$ *(kN)*	*% Diff.*
102 × 102 × 6·4	40·6	223·5	223·6	0·0
152 × 152 × 6·4	57·2	175·3	170·4	2·8
152 × 152 × 6·4	57·2	175·3	169·1	3·6
152 × 152 × 6·4	57·2	175·3	174·3	0·6
152 × 152 × 9·5	58·4	547·5	507·2	7·3
203 × 203 × 9·5	73·7	434·4	396·8	8·7

4.2.3 Mode IV tests

The longest columns that were tested in the short column range were those corresponding to mode IV, shown in Figs 6–9, of the theoretical curves. For the theoretical mode IV lengths, the buckled flange will have a shape corresponding to four full wavelengths. Figure 16 shows the hyperbolic measurements taken during the test of the 152 mm × 152 mm × 6·4 mm (6″ × 6″ × 1/4″) wide flange I-beam and the resulting regressed line. Table

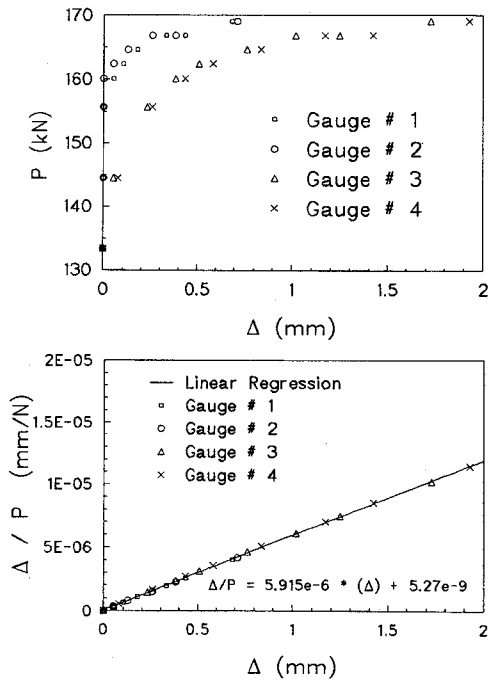

Fig. 15. Mode III hyperbolic and linearized measurements for the 152 mm × 152 mm × 6·4 mm (6″ × 6″ × 1/4″) WF I-beam.

4 shows the length, theoretical buckling load, experimental buckling load (inverse of slope) and the percentage difference between the theoretical solution and the experimental results. As seen from Table 4, all percentages are rather large (13–24%) and all loads are below the theoretical prediction. These large differences may be a result of interaction between long and short column ranges as shown by Tomblin.[16] The possibility of interaction can be visualized in Figs 6–9 from the length of the column in mode IV being close to the column length at the intersection of the local and Euler buckling curves.

4.3 Experimental observations

During the testing and data reduction procedure, various observations were made as follows:

(1) All gauges had small movements from the initial application of load and then stabilized at a load ($P \leq 111$ kN) until flange buckling occurred. The stable range was large (133 kN to 445 kN).
(2) In several cases one flange buckled before the other, which may be

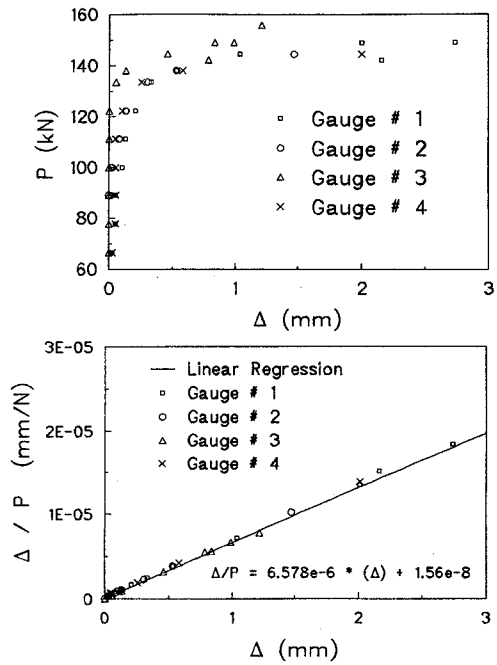

Fig. 16. Mode IV hyperbolic and linearized measurements for the 152 mm × 152 mm × 6·4 mm (6″ × 6″ × 1/4″) WF I-beam.

TABLE 4
Resulting Experimental Local Buckling Loads for Mode IV Tests

Section (mm)	*Length (cm)*	P_{theory} *(kN)*	$P_{exper.}$ *(kN)*	*% Diff.*
102 × 102 × 6·4	54·6	223·5	180·8	19·1
102 × 102 × 6·4	54·6	223·5	222·4	5·0
152 × 152 × 6·4	76·2	175·3	143·0	18·4
152 × 152 × 6·4	76·2	175·3	148·8	15·1
152 × 152 × 6·4	76·2	175·3	161·8	7·7
152 × 152 × 6·4	76·2	175·3	152·0	13·3
152 × 152 × 9·5	77·5	547·5	455·3	16·8
203 × 203 × 9·5	100·3	434·4	329·2	24·2

caused by imperfections existing in that flange. However, this phenomenon did not affect the value of the critical load due to the use of the data reduction method proposed herein.

(3) When flange buckling occurred, all gauges had movement without extra addition of load. Thus, possible human error in gauge readings may exist. However, the dispersion of values and correlation with theoretical prediction are very good.

(4) In the case of the 152 mm × 152 mm × 9·5 mm (6″ × 6″ × 3/8″) and the 203 mm × 203 mm × 9·5 mm (8″ × 8″ × 3/8″) sections, only a few gauge readings could be obtained. This was due to the fact that once buckling occurred, the column experienced loud cracking and large gauge movements. This, in combination with the high load, made the total failure of the column progress very quickly and made manual reading of the gauges difficult.
(5) During the testing procedure, in the case in which no changes in the gauge readings are obtained (i.e., gauge positioned at an inflection point), the gauge readings must be neglected in the regression analysis. However, during all the testing done on all the FRP sections, this was encountered only twice.
(6) Mode IV tests produced the highest degree of error between experimental loads and theory. These discrepancies are due to interaction existing between the local and global buckling modes as shown by Tomblin.[16]
(7) Although the proposed method accurately determines the local buckling of the flange, all FRP columns tested exhibited a certain degree of post-buckling stiffness. Hence, the total ultimate strength of the column is greater than that predicted by just the local buckling analysis. However, it should be noted that in most cases, permanent damage of the section occurred via internal cracks, delamination, etc., as was evident when the column was reloaded.
(8) Due to the instrumentation employed, no measurement of the post-buckling wavelength was possible.

Figures 6–9 show the experimental load obtained plotted with the theoretical curves for each section. As seen from these figures, good agreement with the elastically restrained theoretical load exists.

5 CONCLUSIONS

The local flange buckling load obtained experimentally appears to be in good agreement with the theoretical loads for each wide flange I-beam section tested. As shown in Tables 2 and 3, all percentage differences between the theoretical and experimental loads are below 11%. The large percentage differences experienced in the mode IV test reported in Table 4 should be further investigated. Measurements of the post-buckling wavelength should be attempted.

A novel method to obtain the local buckling load based on Southwell's method was developed. As can be seen in the linearized Δ–Δ/P plots, all

measurements fall close to the regressed straight line with very little data scatter. Thus, by using this method in local buckling tests of pultruded beams, one can account for the material imperfections common in the pultrusion manufacturing process.

ACKNOWLEDGEMENTS

This research was supported by Creative Pultrusions, Inc. The materials used in this investigation were supplied by the same company. Their collaboration is gratefully acknowledged. The help of technicians in the College of Engineering at West Virginia University is also appreciated.

REFERENCES

1. *Creative Pultrusions Design Guide*. Creative Pultrusions, Inc., Pleasantville Industrial Park. Alum Bank, PA 15521, 1988.
2. Chajes, A., *Principles of Structural Stability Theory*. Prentice-Hall, Englewood Cliffs, NJ, 1974.
3. Jones, R. M., *Mechanics of Composite Materials*. Hemisphere Publishing Corporation, New York, 1975.
4. Tsai, S. W. & Hahn, H. T., *Introduction to Composite Materials*. Technomic Publishing Co., Lancaster, PA, 1980.
5. Barbero, E. J., Pultruded structural shapes — from the constituents to the structural behavior. *SAMPE J.*, **27**(1) (1991) 25–30.
6. Barbero, E. J. & Raftoyiannis, I. G., Buckling analysis of pultruded composite columns. In *Impact and Buckling of Structures*, ed. D. Hui & I. Elishakoff, ASME, AD-Vol. 20, AMD-Vol. 114, 1990, 47–52.
7. Bleich, F., *Buckling Strength of Metal Structures*. McGraw-Hill, New York, 1952.
8. Cheung, Y. K., *Finite Strip Method in Structural Analysis*. Pergamon Press, New York, 1976.
9. Vakiener, A.R., Zureick, A. & Will, K. M., Prediction of local flange buckling in pultruded shapes by finite element analysis. *Advanced Composite Materials*, ASCE Publications, 1991, pp. 302–12.
10. Yuan, R. L., Hashen, Z., Green, A. & Bisarnsin, T., *Fiber-reinforced plastic composite columns*. In *Advanced Composite Materials in Civil Engineering Structures*, ed. S. L. Iyer, ASCE, Las Vegas, NV, 31 January–1 February 1991, pp. 205–11.
11. Southwell, R. V., On the analysis of experimental observations in problems of elastic stability. *Proc. Roy. Soc. London (A)*, **135** (1932) 601–16.
12. Southwell, R. V., *Theory of Elasticity*. Oxford University Press, London, 1941.
13. Tsai, W. T., Note on Southwell's method for buckling tests of struts. *J. Appl. Mech.*, **53** (1986) 953–4.

14. Fisher, H. R., An extension of Southwell's method of analyzing experimental observations in problems of elastic stability. *Proc. Roy. Soc. London (A)*, **144** (1934) 609–30.
15. Raftoyiannis, I. G., *Buckling of Pultruded Composite Columns*. MSCE Thesis, West Virginia University, WV, 1991.
16. Tomblin, J. S., *A Universal Design Equation for Pultruded Composite Columns*. MSME Thesis, West Virginia University, WV, 1991.